Received 18 June 2019; revised 3 September 2019; accepted 4 September 2019. Date of publication 9 September 2019; date of current version 30 September 2019. The review of this article was arranged by Editor M. J. Kumar.

Digital Object Identifier 10.1109/JEDS.2019.2940086

Simulation-Based Model of Randomly Distributed Large-Area Field Electron Emitters

JOHANNES BIEKER [1], RICHARD G. FORBES [2] (Senior Member, IEEE), STEFAN WILFERT [3], AND HELMUT F. SCHLAAK [1] (Life Member, IEEE)

1 Laboratory Microtechnology and Electromechanical Systems (M+EMS), Technische Universität Darmstadt, 64283 Darmstadt, Germany
2 Advanced Technology Institute, University of Surrey, Guildford GU2 7XH, U.K.
3 GSI Helmholtz Centre for Heavy Ion Research, Commons - Vacuum Systems, 64291 Darmstadt, Germany

CORRESPONDING AUTHOR: J. BIEKER (e-mail: j.bieker@emk.tu-darmstadt.de)

The research at Technische Universität Darmstadt was supported in part by the German Federal Ministry of Education and Research under Project 05P18RDRB1, and in part by the GSI Helmholtzzentrum für Schwerionenforschung in Darmstadt, Germany, within the Research and Development Project 500475 in frame of FAIR Phase-0.

ABSTRACT With a large-area field electron emitter (LAFE), it is desirable to choose the spacings of individual emitters in such a way that the LAFE-average emission current density and total current are maximised, when the effects of electrostatic depolarization (mutual screening) are taken into account. This paper uses simulations based on a finite element method to investigate how to do this for a LAFE with randomly distributed emitters. The approach is based on finding the apex field enhancement factor and the specific emission current for an emitter, as a function of the average nearest neighbor spacing between emitters. Using electrostatic simulations based on the finite element method, the influence of neighboring emitters on a reference emitter being placed at the LAFE centre is investigated. Arrays with 25 ideal (identical) conical emitters with rounded tops are studied for different emitter densities and applied macroscopic fields. A theoretical average spacing is derived from the Poisson Point Process Theory. An optimum average spacing, and hence optimum emitter density, can be predicted for each macroscopic field.

INDEX TERMS Field electron emission, large area field emitters, micro-nano-integration, modelling, simulation.

I. INTRODUCTION

Field electron emitters are important for vacuum electron sources and already find applications, e.g., as cathodes in vacuum gauges [1]–[3] or X-Ray sources [4], [5]. For high current applications, large-area field emitters (LAFEs) are commonly used.

Detailed field electron emission (FE) measurements of cathodes with in-situ deposited gold nanocones have been presented recently [6]. These LAFEs are fabricated using asymmetric etching of low-cost, ion-track polymer membranes and subsequent electro-deposition. Due to the fabrication process of the membranes, the ion tracks are randomly distributed on the foil, leading to nanocones with the same distribution, as shown in Fig. 1. It is planned that these cathodes will be used in an ionization vacuum gauge, which needs a stable total emission current in the order of some hundred microamperes [2]. There are two main options to increase and thus optimize the total emission current of the LAFE: decreasing the emitter apex radii to obtain higher field enhancement, or alternatively optimizing the emitter density and therefore the electrostatic interactions between the emitters. Decreasing the emitter apex radii is technologically not easy due to the fabrication process. Thus attention here is concentrated on optimizing the emitter density.

A parameter of particular interest is an emitter's apex field enhancement factor (FEF) γ. In the context of a model in which an emitter stands on one of a pair of adequately separated parallel planar plates, the emitter's apex field enhancement factor (FEF), γ, is defined as the quotient

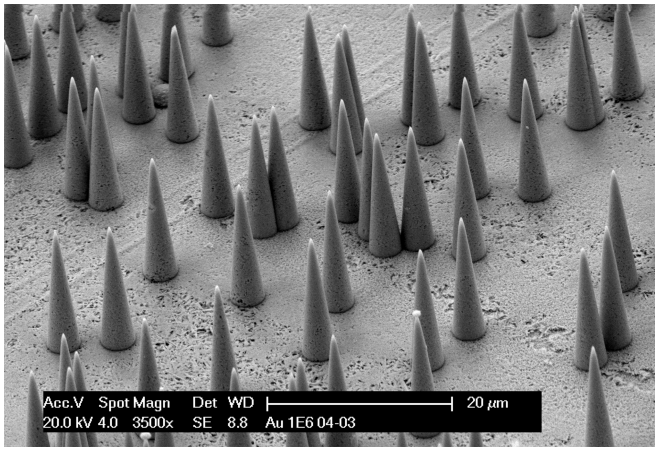

FIGURE 1. SEM image of randomly distributed gold nanocones (with a mean density of 1 × 10^6 cones/cm^2) fabricated using asymmetrically etched, low-cost polymer membranes as templates and filling the pores via electrodeposition.

F_a/F_M of its apex field F_a to the mean (or "macroscopic") field F_M between the plates.

Complete simulations of LAFEs are time-consuming due to the necessary multi-scale modelling and meshing of small emitting structures in the presence of larger electrodes. Hence, normal practice is to consider separately (a) the emission from a single isolated emitter, and (b) interactions between emitters due to electrostatic depolarization effects (usually described as "screening" or "shielding").

Single-emitter models analysed include the "hemisphere-on-cylindrical-post" model, the "hemi-ellipsoid" model, and the "parabolic tip" model (e.g., [7]–[9]). Interactions between emitter pairs, and in regular emitter arrays, have been investigated (e.g., [10], [11]). Recently, line-charge models (LCMs) have been used to describe both single emitters and emitter arrays [12]–[15]. Further, in an attempt to represent fabrication inhomogeneities, emission from LAFEs with a Gaussian distribution of apex field enhancement factors has been modelled [16].

However, there is also a need for models that treat electrostatic depolarization effects in arrays where the emitters are randomly distributed. In particular, there is a need to predict the optimum emitter density, i.e., the mean number of emitters per unit area, in order to be able to maximize the total emission current and hence the efficiency (in applications) of a randomly distributed LAFE. So far, there are very few such models that do this.

Very recently, Biswas and Rudra [17] published an analytical model for the emission of randomly distributed emitters based on a LCM.

In older works, Read and Bowring [18] investigated the distribution of field enhancement factors for both ordered and randomly distributed CNT arrays, using simulations based on a finite element method (FEM). However, to evaluate and optimize the performance of arrays with different emitter densities, it is necessary to investigate the behaviour of the macroscopic ("LAFE average") emission current density (ECD).

II. PHYSICAL BACKGROUND

The aim of this work is to determine the optimum emitter surface density for a very large (effectively infinite) random emitter array. However, currently it is computationally impracticable to carry out FEM simulations for very large arrays, and one needs to work instead with a random array (or "cluster") of finite size, say N emitters. In our case, this is taken as an array of $N = 25$ emitters, assumed to be drawn from a population with average emitter surface density σ. Thus, the average area per emitter ("emitter footprint") is $1/\sigma$.

One of these emitters (designated the reference emitter) is regarded as an emitter that is typical of emitters in an infinite array, and is placed at the center of a so-called footprint circle of area N/σ, and hence of footprint radius $r_{\text{foot}} = (N/\pi\sigma)^{\frac{1}{2}}$. Numerical simulations on this central reference emitter, when treated as an isolated single emitter, lead to a value γ_1 for its apex FEF. The presence of other emitters in the very large random array will cause depolarization effects, usually called "mutual shielding" or "screening" [10], [11], [19], and hence a reduction in the apex FEF. The total depolarization effect can be considered as the result of effects of three kinds.

1) Depolarization effects associated with a finite regular array of N emitters all with emitter footprints of $1/\sigma$.
2) Changes (normally an increase) in depolarization effects due to randomisation of the array of N emitters.
3) Depolarization effects due to the remaining emitters in the very large array; these are called here the distant emitters.

The reason why randomization normally leads to an increase in depolarization effects in comparison to regular arrays is as follows. Except at very small emitter separations (which are not of significant interest in the present context), the strength of the depolarizing effect depends on the emitter separation d as d^{-n} where $1 \leq n \leq 3$, (n becomes equal to 3 in the limit of large separations [11], [20]). Hence, an emitter in the regular array that is moved "inwards" (towards the central emitter) by a small distance δ strengthens the depolarization by an amount that is greater than the amount by which the depolarization is weakened if an equivalent emitter is moved outwards by a small distance δ. Hence, on average, the overall effect of randomization is to expected to strengthen depolarization.

It is relatively easy to investigate effects (1) and (2) by using electrostatic simulations based on FEM. But this leaves open the question of how to deal with effect (3). Our view is that, at present, it is not clearly known how best to deal with depolarization effects due to the distant emitters, and that detailed research into this issue is required. The present paper aims to be an exploratory paper that make a preliminary investigation of the combined influence of effects (1) and (2) above, leaving exploration of effect (3) to future work.

TABLE 1. Geometrical parameters used in the FEM simulation.

Geometrical parameter	Symbol	Value
Emitter base radius	r_{base}	1.75 μm
Emitter apex radius	r_{tip}	25.0 nm
Emitter height	h	24.0 μm
Cathode-anode-distance	d_{CA}	120.0 μm
Emitter surface density	σ	variable
Av. NN separation	$\overline{d}$	dep. on σ
Av. spacing	$\overline{s}$	$\overline{d}/h$
Footprint circle area	A	N/σ
Footprint circle radius	r_{foot}	$\sqrt{N/\pi\sigma}$
Applied potential difference	U	variable
Simulation box radius	r_{sim}	500 μm

TABLE 2. List of used quantities and constants.

Quantity or constant	Symbol	Value and/or unit, ref.
Reference emitter current	I_1	A
Emitter density	σ	1/cm^2
FEF	γ	
FN-constants	a_{FN}	$1.54 \cdot 10^{-6}$ A $\cdot$ eV/V^2, [25]
	b_{FN}	$6.83 \cdot 10^{9}$ V/(eV$^{\frac{3}{2}} \cdot$ m), [25]
Local electric field	F	V/m
Macro. appl. elec. field	F_{M}	V/m
Geometry factor	g	
Local ECD	J_{L}	A/m^2
Macro. ECD	J_{M}	A/m^2
SN-barrier functions	t_{F}	see [25]
	v_{F}	see [25]
work function (Au)	Φ_{W}	4.82 eV [26]

The procedure will be applied to LAFEs fabricated using conically shaped emitters with hemispherical tips, as described earlier. However, it also can be used for any geometry of field electron emitters.

III. MODELLING

This section uses the parameters shown in Tables 1 and 2. Its structure is as follows.

First, we describe the general geometrical and statistical arrangements, and give information about the finite element methods (FEM) used in the electrostatic simulations.

Next, we discuss the modelling of a single isolated emitter, determine a value for the related apex FEF γ_1 and derive a formula for the related emission current I_1 as a function of the apex field F_a. The situation in an array is then considered.

After this, statistical/electrostatic simulations and analysis are carried out, in order to make empirical determinations of the average nearest-neighbour (NN) distance $\overline{d}_{\text{NN}}$ between (the symmetry axes of) the central reference emitter and the nearest emitter, and of the corresponding average apex FEF $\bar{\gamma}$ for the central reference emitter. These distances $\overline{d}_{\text{NN}}$ are used to define dimensionless average NN "spacings" $\bar{s}$ by the formula $\bar{s} = \overline{d}_{\text{NN}}/h$. The simulations are carried out for a set of five emitter surface densities, and for two values of F_{M}. In each case, at least 14 different random emitter placements are used in order to determine the average values $\bar{s}$ and $\bar{\gamma}$.

In addition, thereby demonstrating consistency, these average NN distances can be compared with a theoretical prediction of Poisson Point Process Theory (PPPT), that holds for sufficiently large emitter arrays as it describes infinitely large distributions without a border.

The results are then used in a regression analysis that derives a formula for $\bar{\gamma}$ as a function of $\bar{s}$. For each given macroscopic field, this formula is then used to derive information about how the macroscopic ("LAFE average") emission current density is predicted to vary with average NN spacing $\bar{s}$ (and hence with emitter surface density). From this, a predicted maximum current density for field F_{M}, and a related optimum average emitter surface density, can be derived.

The following sections discuss these results.

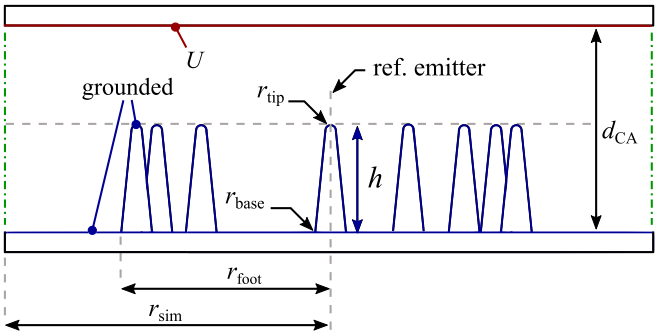

FIGURE 2. Illustration in cross-sectional view of the geometrical parameters used to simulate the FEF and the emission current of an emitter within an array of randomly distributed emitters. The boundary conditions used are also shown. The emitter surfaces as well as the bottom surface of the cathode are grounded. The electrostatic potential *U* is applied to the lower surface of the anode. The footprint and therefore the array size are characterized by the radius r_{foot}. The maximum r_{foot} used in the simulation is 282 μm, corresponding to an emitter density of 10^4 emitters/cm^2. The radius r_{sim} of the simulation box is kept constant at 500 μm. The green dashed lines illustrate the borders of the simulation box at which the electrostatic field is tangential to the sides (or perpendicular to the normal vector of the sides).

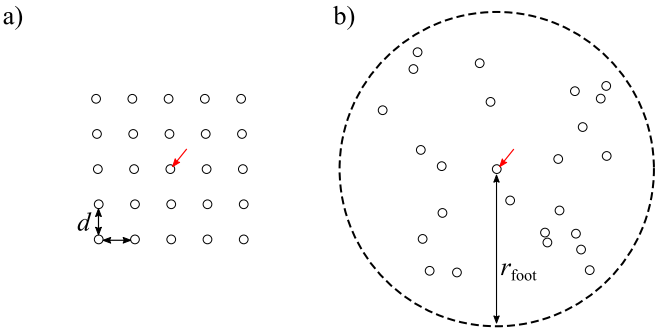

FIGURE 3. Top view on a regular square array and an array with randomly distributed emitters. The FEF and the emission current of the emitter at the array center - marked with an arrow - are observed.

A. SIMULATION ARRANGEMENTS

The geometrical parameters for each identical rounded conical emitter used in the simulation are given in Table 1 and are based on the actual parameters of the fabricated emitters, as shown in Fig. 1. We consider an array of 25 emitters being placed on one of a pair of parallel, circular planar plates, as

shown in cross-sectional view in Fig. 2. The reference emitter is placed at the plate center. The axes of symmetry of the other 24 emitters are placed randomly (as described below) within a "footprint circle" of area $A = 25/\sigma$, where σ is the selected emitter surface density. The circle has a radius $r_{\text{foot}} = \sqrt{A/\pi}$. Fig. 3 b) illustrates one such placement.

The studied densities are 10^4, 5×10^4, 10^5, 5×10^5 and 10^6 emitters per cm^2 with corresponding values of r_{foot} lying between 28.2 μm and 282 μm. The radius r_{sim} of the cylindrical simulation box is kept constant at 500 μm. The cathode-to-anode plate separation d_{CA} is chosen to be 120 μm, which is equal to five times the total height h of each emitter. This ratio should be large enough for anode-proximity effects to be disregarded [21], [22].

Depending on the precise placements of nearby emitters, the apex FEF of the central reference emitter and hence its specific emission current I_1 will change between different placements. As discussed in Section II, there is an issue as to how many emitters need to be considered in order to get a reliable result for the average apex FEF and the specific emission current.

For a regular square array, Harris *et al.* consider that sixth and higher-order nearest neighbours do not contribute significantly to depolarization effects at the central emitter [23]. This statement implies that, for square-shaped arrays, considering arrays of 25 emitters delivers representative results, compare Fig. 3 a). The assumption has been made here that taking 25 as the number of simulated emitters is sufficient in all cases (also for random arrays, see discussion later.) This number is kept fixed for all simulations. There is also an issue as to how many placements, for given values of σ and chosen macroscopic field F_{M}, are needed to make a valid estimate for the reference emitter's apex FEF. As indicated above, we have used at least 14 different emitter arrangements in each case.

Simulations are carried out using MATLAB and CST EM Studio.

To obtain a homogeneous distribution of emitters per area on a circular area, a random generator implemented in MATLAB is used, delivering random numbers $p_n \in [0, 1]$, and polar coordinates (r, φ) of the emitters are defined by [24]

$$r_i = \sqrt{p_{i,1}} \cdot r_{\text{foot}} \tag{1}$$

$$\varphi_i = 2\pi \cdot p_{i,2}. \tag{2}$$

As already noted, the reference emitter is always located at the array center, but for each of the other 24 emitters a pair of coordinates is created by this procedure. Based on this list of coordinates, emitters are positioned in the parallel plate configuration in CST-Studio via a VBA-interface from MATLAB, compare Fig. 3 and Table 1. An exemplary array is shown in Fig. 4 a).

The electrostatic solver of CST EM Studio is controlled via a VBA interface from MATLAB and uses FEM to simulate the electrostatic potential distribution for this configuration. The anode-to-cathode potential differences used are 800 V ($F_{\text{M}} \approx 6.66$ MV/m) and 1000 V ($F_{\text{M}} \approx 8.34$ MV/m).

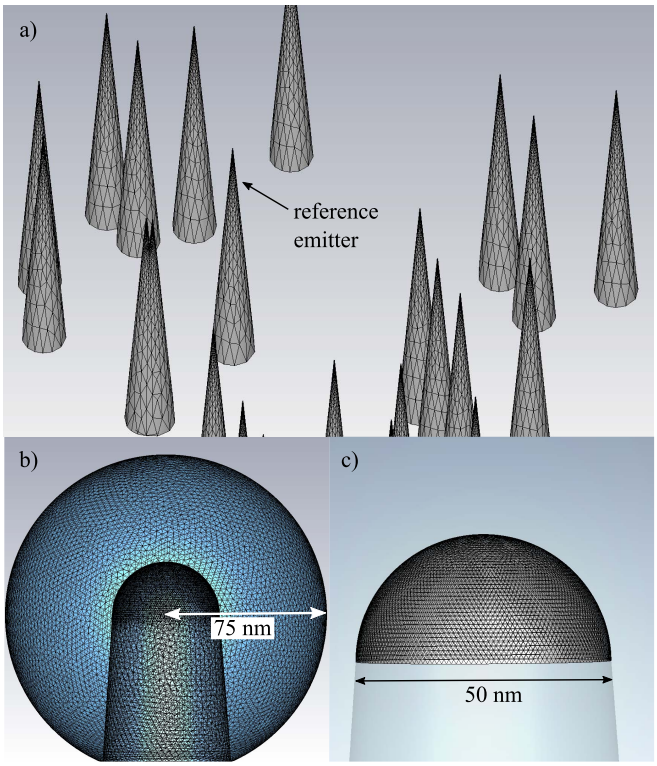

FIGURE 4. **a) An exemplary simulated emitter array containing 25 conical emitters with spherical tips is shown. In this example, the emitter density is 10^6 emitters/cm^2. For each of the 5 simulated emitter densities, at least 14 different emitter distributions are simulated and analysed, especially the electrostatic field at the reference emitter tip located at the array center. b) To avoid self-intersections of the meshes of the spherical tip and the conical body of the emitter, the space around the tips is fine-meshed to a radius of 3 times the tip radius (i.e., 75 nm). c) Detailed view of the surface mesh of a single tip with a radius $r_{\text{tip}} = 25$ nm. The electrostatic field is mapped around the reference emitter tip at a distance from 0.1 nm to the emitter surface.**

To analyze the electrostatic field later on, a pointlist of coordinates on a hemisphere around the emitter tips at a distance of 0.1 nm from the emitter surface is created and transferred to CST EM Studio. As it is usual in simulations of this kind, the emitter is (for simplicity) modelled as a perfect classical conductor with a work function that is the same at all points on the conductor surface. This allows us to assume that the electrostatic potential is the same at all points immediately outside the model surface.

Meshing of the setup has to be done carefully, as the whole setup has geometries interacting at up to 2 orders of magnitude: the emitter tips have a radius of 25 nm and the diameter of the simulated array is in the order of micrometer. Therefore, the space around the emitter tips at a radius of up to 75 nm is particularly fine-meshed, compare Fig. 4 b). In Fig. 4 an exemplary simulated emitter array is shown, as well as detailed views of the mesh around the emitter tips and on the emitter surface.

After meshing and solving, CST EM Studio returns the values of the electrostatic field at the pointlist coordinates to MATLAB.

B. ELECTROSTATIC INTERACTION BETWEEN EMITTERS

To model the field emission characteristics of the reference emitter (namely its field enhancement factor γ and specific emission current I_1) as a function of the emitter distribution and the applied electrostatic field, the situation at the reference emitter apex will be discussed. First, the situation for an isolated single emitter is outlined. Based on this, the situation of the reference emitter in an array is considered.

For a given value of macroscopic field F_M, FEM simulation gives local electric field (F) values on the surface of an isolated single emitter, and hence the values of its apex local field $F_a = \gamma_1 F_M$ and apex FEF γ_1. For our emitters γ_1 is found to be 475.9.

A formula for the current I_1 from this emitter can be obtained by integrating the local emission current density (LECD) $J_L(F)$ over the surface of the emitter and writing the result in the form

$$I_1 = A_n \cdot J_a \tag{3}$$

where J_a [$:= J_L(F_a)$] is the apex LECD and A_n is the emitter's notional emission area, which is defined by this equation. For the LECD, Murphy and Good's zero-temperature FE equation (MG FE equation) from 1956 is used [27]. It reads

$$J_L(F) = \frac{a_{FN} \cdot F^2}{\Phi_W t_F^2} \cdot \exp\left(-b_{FN} \cdot v_F \cdot \frac{\Phi_W^{\frac{3}{2}}}{F}\right) \tag{4}$$

with the Fowler-Nordheim constants a_{FN} and b_{FN} as given in Table 2, t_F and v_F as appropriate particular values of the Schottky-Nordheim barrier functions [25], [28], [29] and F as the local barrier field at the emitter surface. In this case, a work function $\Phi_W = 4.82$ eV for gold was used to fit the model to the fabricated emitters [26]. Strictly, equation (4) is only applicable for metallic emitters. For example, carbon-based emitters, the MG FE equation should (in principle) be modified as suggested in [29].

In the present work, instead of A_n it is more convenient to use a "geometry factor" g (also called a "notional ratio factor" [30], or a "notional apex efficiency") defined by

$$g = \frac{A_n}{2\pi r_{tip}^2} = \frac{I_1}{J_a \cdot 2\pi r_{tip}^2}, \tag{5}$$

where r_{tip} is the apex radius of curvature. The parameter g is a function both of the apex field F_a ($= \gamma_a F_M$) and of the emitter shape [30]. For some tip geometries, for example hemispherical and hemi-ellipsoidal protrusions, analytical expressions exist for $g(F_a)$ [30]. However, Jensen suggests that the geometry factor can be approximated with a linear function for other geometries as well [30]. This assumption is adopted at this point, although the form of the underlying function for g is an issue of current research. However, the linear approximation seems to be a valid first estimation.

Using the isolated-emitter simulation results for two different values of F_M (namely $6.66\,V/\mu m$ and $8.33\,V/\mu m$), and carrying out surface integrations to derive values for I_1, yields the results $g = 0.21 \pm 0.02$ for $F_a = \gamma_1 \cdot F_M = 3.17\,V/nm$ and $g = 0.25 \pm 0.02$ for $F_a = 3.96\,V/nm$. These results enable the following formula to be derived for $g(F_a)$, for emitters of the shape we are using, as an approximation

$$g(F_a) = 0.065\,\frac{nm}{V} \cdot F_a. \tag{6}$$

For regular emitter arrays, it is common to use the dimensionless parameter s (called here the "emitter spacing", or briefly "spacing"), which equals the distance between emitter axes, normalized by the height h of the emitters [11], [12], [20].

Recent publications have shown that for spacings $s > 1.5$ the reduction of the apex FEF follows a s^{-3}-decay [11], [20], which has also been derived from physical laws. But so far a suitable, physically derived fit-function $\gamma(s)$ for spacings below 1.5 is missing. Due to the lack of a fit-function for this technologically interesting regime, commonly the apex FEF is fitted using a phenomenological function $\gamma(s)$. A fit function previously used by Harris *et al.* [12] is

$$\gamma(s) = \gamma_1 \cdot \left(1 - \exp\left(a \cdot s^c\right)\right). \tag{7}$$

Here, γ_1 is the apex FEF for an isolated single emitter, and $\gamma(s)$ is the apex FEF as reduced by the depolarization effects that occur when the emitter is part of an array with spacing s. The parameters a and c are fitting constants. For a regular square array, a has been estimated as around -2.31 by Jo *et al.* [31], but Harris *et al.* [23] using LCMs find a value of -1.45. Harris *et al.* also interpret c as providing a further degree of freedom for the fit.

The current task is now to find a suitable fit-function which holds for random arrays and describes the average apex FEF γ of the reference emitter appropriately. At this point, we assume that equation (7) can be taken as a fit function to describe the reduction of an average apex FEF $\bar{\gamma}(\bar{s})$ as a function of the average spacing $\bar{s}$ to the NN emitter instead. But, one main aspect that has to be considered is that the spacing s of an ordered array is not equal to the spacing of NN emitters in randomly distributed arrays. Therefore, a detailed look will be taken on the average NN spacing $\bar{s}$.

C. EVALUATION OF NEAREST-NEIGHBOR SPACINGS

What the statistically based simulations directly provide, for the five values of emitter surface density used, are average values of NN spacings and the corresponding values of average apex FEF for the reference emitter.

Our five calculated values of $\bar{s}$ are shown in Fig. 5. The error limits shown represent the standard errors of the average NN spacing $\bar{s}$.

These empirical results can be compared with theoretical mean NN spacings s_{mean} derived from Poisson Point

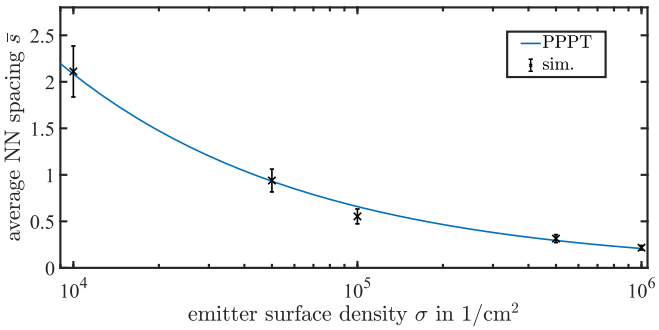

FIGURE 5. Comparison of average NN spacings of LAFEs obtained theoretically and by FEM simulation for emitter surface densities between 10^4 and 10^6 emitters/cm^2.

Process Theory (PPPT). This theory neglects border effects and therefore holds only for sufficiently large cathodes [32]. Qualitatively, it is to be expected that border effects, although important for very-small radius LAFEs, will decrease in relative importance as LAFE size increases.

According to PPPT theory, the probability distribution function for NN separation, $f_{d_{\mathrm{NN}}}$ is

$$f_{d_{\mathrm{NN}}}(\sigma, d) = 2\pi\sigma \cdot d \cdot e^{-\sigma\pi d^2}. \tag{8}$$

In general, the predicted mean spacing can be derived via

$$s_{\mathrm{mean}} = \frac{1}{h} \cdot \int_0^\infty d \cdot f_{d_{\mathrm{NN}}}(\sigma, d)\, \mathrm{d}d. \tag{9}$$

This results in

$$\Rightarrow s_{\mathrm{mean}} = \frac{1}{2 \cdot h \cdot \sqrt{\sigma}}. \tag{10}$$

The surface-density dependence of the parameter s_{mean}, as found by eq. (10), is also shown in Fig. 5.

An important result from Fig. 5 is that our empirical average NN spacing values $\bar{s}$ lie almost exactly on the theoretical mean-spacing curve. This gives us confidence that the use of 14 placements for each surface density σ has been sufficient and also gives us confidence to continue with the discussion here.

Equation (10) can be compared with the equivalent formula for a square array of the same surface density σ, namely

$$s_{\mathrm{sq.ar.}} = \frac{1}{h \cdot \sqrt{\sigma}}. \tag{11}$$

This shows that, for the random array, the typical NN spacing is predicted to be half of the square array.

D. DETERMINATION OF THE AVERAGE FEF AS A FUNCTION OF THE AVERAGE SPACING

As described in Section III-B, equation (7) will be used to describe the average apex FEF $\bar{\gamma}$ for the central reference emitter as a function of the average NN spacing $\bar{s}$. Therefore, the fitting parameters a and c have to be determined using the average apex FEF $\bar{\gamma}(\bar{s})$ of the reference emitter obtained from the FEM simulations. The given formulas are transformed so that linear regression is applicable. This allows a better determination of the values for a and c.

First a "fractional reduction in apex FEF" ρ is defined and given by

$$\rho(\bar{s}) := \frac{\gamma_1 - \overline{\gamma}(\bar{s})}{\gamma_1} = \exp(a \cdot \bar{s}^c). \tag{12}$$

ρ is positive and less than unity (compare, e.g., [11]); hence $\ln\rho$ is negative. Thus, this leads to

$$\ln(\rho) = a \cdot \bar{s}^c \tag{13}$$

$$\Rightarrow \ln(-\ln(\rho)) = \ln(-a) + c \cdot \ln(\bar{s}). \tag{14}$$

Defining $y = \ln(-\ln(\rho))$ and $x = \ln(\bar{s})$, the fitting parameters a and c are then simply derived from the intercept and the slope of the fitted straight line. For both cases this fitting procedure worked well in a range of spacings between 0.25 and 4, which is the region of interest here. For spacings beyond this range a different fit function is necessary, because the error between the data and the fit is increasing [20]. In Figure 6 a) one can see the fitting for the obtained simulation data. We found $a = (-2.41 \pm 0.07)$ and $c = (0.74 \pm 0.03)$. Figure 6 b) shows how the resulting mean FEF $\overline{\gamma}$ varies as a function of the average spacing $\bar{s}$, with the five simulation values superimposed.

E. DEPENDENCE OF MACROSCOPIC CURRENT DENSITY ON NN SPACING

Now that we have a formula for $\bar{\gamma}(\bar{s})$, and hence for $F_{\mathrm{a}}(\bar{s})$, equation (5) earlier can be used to model the average specific emission current $\bar{I}_1(F_{\mathrm{M}}, \bar{s})$ as a function of macroscopic field F_{M} and of NN spacing $\bar{s}$ (and hence of emitter surface density σ). We make the reasonable assumption that, for the average NN spacings of interest in this paper, the formula given in equation (6) can used for all average NN spacings, using only the values of average apex FEF $\bar{\gamma}$ (and hence F_{a}) determined from the simulations as a function of $\bar{s}$. One then uses

$$\bar{I}_1(\bar{s}, F_{\mathrm{M}}) = 2\pi r_{\mathrm{tip}}^2 \cdot J_{\mathrm{a}}(F_{\mathrm{a}}) \cdot g(F_{\mathrm{a}}). \tag{15}$$

This yields the continuous curve shown in Fig. 6 c). Also shown in Fig. 6 c) are some individual average-current values for the central reference emitter, calculated as part of the main set of simulations, rather than via (15). These are close to, but lie slightly above, the continuous curve. This shows that our procedures are basically consistent, but that some very small numerical discrepancies remains. Given that this is intended as a basic exploratory paper, we think these small discrepancies not worth investigating here.

The resulting dependence on $\bar{s}$ is presented in Fig. 6 c) for an applied voltage of $U = 1000$ V, with the five simulation results superimposed.

The macroscopic ("LAFE average") current density J_{M} will also be a function of F_{M} and of $\bar{s}$ (and hence of σ) and is given by the product of the average specific emission current $\bar{I}_1$ and the emitter density σ:

$$J_{\mathrm{M}}(\bar{s}, F_{\mathrm{M}}) = \sigma \cdot \bar{I}_1(\bar{s}, F_{\mathrm{M}}). \tag{16}$$

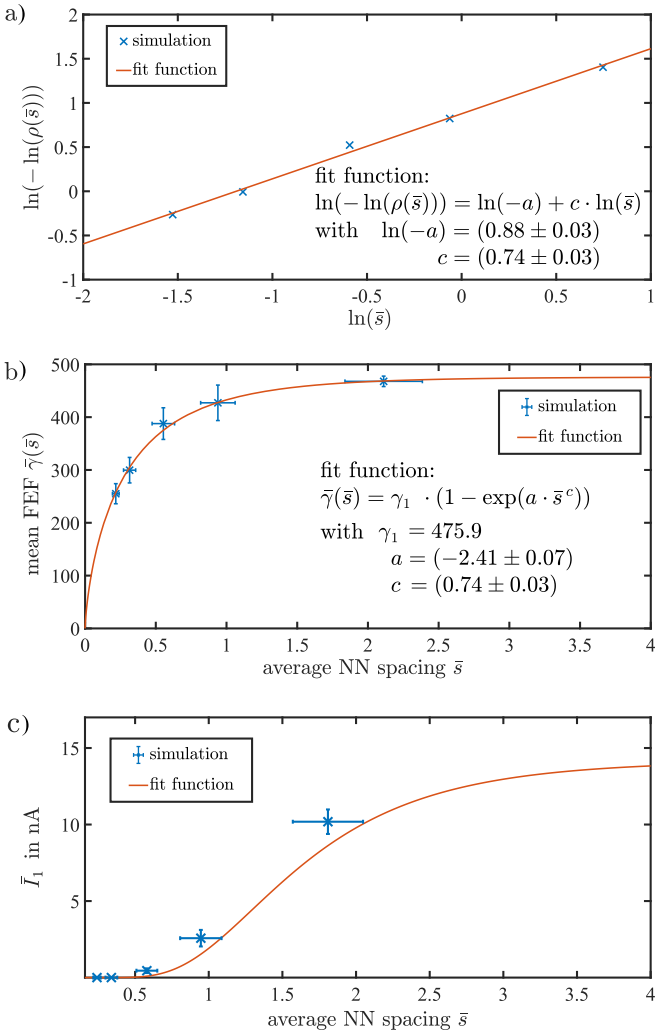

FIGURE 6. **a) Ordinary linear regression of ln($\bar{s}$) and ln(− ln(ρ)) to determine the fitting parameters *a* and *c*, compare equations (12) to (14). b) Results for the mean FEF $\bar{\gamma}$ as a function of the average NN spacing $\bar{s}$ to the second emitter. The fit function is derived from equation (7). $\gamma_1 = 475.9$ was found by simulations on a single isolated emitter. The shown error bars represent the standard errors of the mean values. c) Results for the average specific emission current $\bar{I}_1$ as a function of average NN spacing $\bar{s}$. The model function is given in equation (15).**

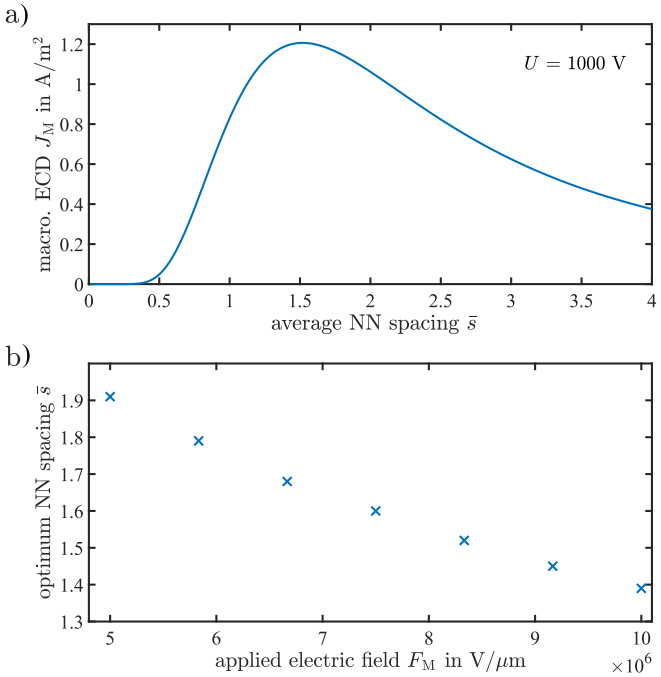

FIGURE 7. **a) Macroscopic ECD J_M as a function of average spacing $\bar{s}$ for $U = 1000$ V, predicted by the presented model based on PPPT. b) Shift of the optimum average spacing given by the maximum of the ECD for increasing applied electric fields F_M.**

Fig. 7 a) shows, for an electrostatic potential difference of 1000 V (corresponding to $F_M \approx 8.34$ MV/m), how J_M varies with $\bar{s}$. Equation (15) has been used to yield values for J_M. As with large regular arrays, this diagram exhibits a maximum in J_M, in our case at about $\bar{s} = 1.5$.

The formulas for $g(F_a)$ and $\bar{I}_1(F_a)$ derived earlier, together with formula (16) above, can be used to show that the position of the maximum of $J_M(F_M, \bar{s})$ depends on the value of F_M, as shown in Fig. 7 b). This is also in qualitative agreement with results found for ordered arrays [23].

The optimum average spacing for the simulated type of emitter is in the range between 1.4 and 1.9, depending on the applied electric field. Following this and considering the statistical fluctuations, the optimum emitter density is in the range of 1×10^4 to 2×10^4 emitters/cm^2 for the given geometry.

IV. DISCUSSION

As indicated in the introduction, this paper is intended as an exploratory paper relating to the effects of emitter randomization. Our emitters have a different shape from those considered in the earlier papers of Read and Bowring [18] and have a specific shape rather than the general considerations investigated by Biswas and Rudra [17]. However, our results relating to emitter depolarization are qualitatively similar to all the earlier work on random arrays.

Our results show that, as with regular arrays, there is an optimum average NN spacing (or separation) for which the macroscopic current density is a maximum. Biswas and Rudra also found this. However, for a given average emitter surface density this occurs at slightly different NN spacings in regular and random arrays.

For a given average emitter surface density, we can compare the apex FEFs of the central reference emitter for the cases of a random array of 25 emitters and a regular square array of 25 emitters. For the latter case, we used FEM methods similar to those used for the random array. The spacing of the array was varied and the electrostatic field at the apex of the center-placed reference emitter analyzed. The FEF γ was fitted as a function of the spacing s using equation (7). For the given geometry, we found the fit parameters $a = (1.59 \pm 0.06)$ and $c = (0.93 \pm 0.04)$. These values are broadly comparable with those found in previous work on

TABLE 3. Comparison of the reference apex FEF in a square array and in a random array as a function of the (average) emitter surface density.

σ	γ_{rnd}	γ_{sq}	$\Delta\gamma$
1×10^4	468	474	6
5×10^4	427	447	20
1×10^5	394	414	20
5×10^5	296	295	1
1×10^6	252	240	12

regular arrays (e.g., [12]), but differ in detail because the situations considered are not strictly comparable. The results are shown in Table 3. It can be seen that the effect of the randomization is always to increase the amount of depolarization, but that the additional depolarisation seems to be relatively small (in comparison with the depolarization that exists in the regular array).

As far as we can judge, the present exploratory paper yields qualitatively correct and useful results concerning the effects of emitter randomization. However, as far as the prediction of physically and numerically exact results is concerned, a weakness is that there are un-investigated issues relating to the influence of depolarization on the calculation of currents from individual emitters, and hence on the predicted average macroscopic current density. These issues fall into three main kinds.

First, there are effects related to the finite size of the 25-emitter array, when considered as part of a very large random array. Based on the Harris *et al.* statement [23], we have initially assumed that 25 emitters should be sufficient to assess depolarization effects on the central reference emitter, due to other emitters in a large random array. However, as a result of remarks by one of the reviewers, and additional unpublished informal calculations by one of us, we now think that distant emitters in a large array (outside the footprint circle for the 25-emitter array) probably produce significant additional depolarization effects on the central reference emitter. (Though these should be appreciably less than the effects due to the 25 emitters in the footprint circle, when these are considered part of a large random array.) The theory needed for dealing accurately with the influence of these distant emitters looks to be far from straightforward, and our plan is to investigate related issues in future work. However, it is clear that the effect of not considering the distant emitters is to underestimate the amount of reference-emitter depolarization that occurs at the centre of a large random array.

Second, there is an issue of what radius the simulation cylinder needs to be, in order to avoid complications due to the images of the 25-emitter array in the cylinder walls. For a single emitter on the symmetry axis of a cuboid simulation box, this has been a topic of recent research by de Assis and Dall'Agnol [33]. They found that the walls of the simulation box should ideally be at a distance of about 10 times the emitter height, slightly depending on the height of the simulation box. We have taken this into account and ensured that the radius of the simulation cylinder is always greater than the radius of the footprint circle by more than 10 times the emitter height. Nevertheless, it not yet clear whether they may be additional restrictions that apply to the situation of a finite array inside a simulation cylinder. We also point out that, strictly, existing theory applies to cuboid simulation boxes, rather than cylinders.

Third, given that our simulations apply to a finite array that is relatively small, in the sense that the footprint radius is only 2.8 times the NN separation in the related regular square array, there is the influence of "electrostatic edge effects". These arise because, in addition to any effects due to emitter randomization, there will an underlying systematic increase in emitter apex-FEF values as one moves away from the centre of the finite array. For small regular finite arrays, this effect is well known, for example [10], [34].

Both the second and third effects will tend to increase the depolarization acting on the central reference emitter, as compared to the situation that would exist if the 25 emitters were part of a much larger random array. Thus, they tend to offset (but not exactly) the depolarization deficit resulting from the absence of the distant emitters. However, we have no reason to think that the results for a correctly analysed large random array would be qualitatively different from those found in the present numerical work on the 25-emitter random array.

A further depolarization-related effect might result from a statistical production fluctuation that causes a small area of a large array to have anomalously low emitter density, and thus anomalously high current density, thereby creating a "local hot spot". Such effects are not covered by our form of theory, which is based on statistically average behaviour, and is aimed at generating the optimum emitter density in production contexts. A separate form of statistical "hot spot theory" would be useful, in order to assess the likely incidence of such behaviour. To some extent, this has already been developed by Read and Bowring [35]. However, the technological solution to hot-spot problems of this kind, if they are found important, is (as with ordinary integrated circuits) development of efficient forms of post-production testing, with rejection of "out-of-specification" LAFEs.

V. SUMMARY

In summary, in this work a model for LAFEs with randomly distributed emitters has been presented. This model combines a fitting function for FEFs (already used with regular ordered field emitter arrays) with information about average emitter spacing obtained from the distribution of nearest-neighbor separations. It is well known that for regular emitter arrays, the optimum lattice spacing (to obtain maximum LAFE-average current density) depends on the value of the applied macroscopic electric field. We have shown, by means of simulations and modelling, that a similar effect applies to random emitter arrays.

This is a exploratory paper that does not take into account various additional electrostatic depolarization effects. The possible influences of these effects have been qualitatively

discussed. We have found no reason to think that the qualitative conclusions of the present paper will be disturbed when quantitative treatments of these effects become available for emitters with the rounded-cone shape considered here.

ACKNOWLEDGMENT

The authors acknowledge support by the German Research Foundation and the Open Access Publishing Fund of Technische Universität Darmstadt.

REFERENCES

[1] F. Dams *et al.*, "Homogeneous field emission cathodes with precisely adjustable geometry fabricated by silicon technology," *IEEE Trans. Electron Devices*, vol. 59, no. 10, pp. 2832–2837, Oct. 2012.

[2] F. Roustaie, S. Quednau, F. Dassinger, H. F. Schlaak, M. Lotz, and S. Wilfert, "*In situ* synthesis of metallic nanowire arrays for ionization gauge electron sources," *J. Vac. Sci. Technol. B Nanotechnol. Microelectron. Mater. Process. Meas. Phenom.*, vol. 34, no. 2, Mar. 2016, Art. no. 02G103.

[3] A. Basu and L. F. Velásquez-García, "An electrostatic ion pump with nanostructured Si field emission electron source and Ti particle collectors for supporting an ultra-high vacuum in miniaturized atom interferometry systems," *J. Micromech. Microeng.*, vol. 26, no. 12, 2016, Art. no. 124003.

[4] S. Park *et al.*, "A fully vacuum-sealed miniature X-ray tube with carbon nanotube field emitters for compact portable dental X-ray system," in *Proc. Med. Imag. Phys. Med. Imag.*, vol. 10573, Mar. 2018, Art. no. 105732G. [Online]. Available: https://doi.org/10.1117/12.2293472

[5] J. H. Hong, J. S. Kang, and K. C. Park, "Fabrication of a compact glass-sealed X-ray tube with carbon nanotube cold cathode for high-resolution imaging," *J. Vac. Sci. Technol. B*, vol. 36, no. 2, Jan. 2018, Art. no. 02C109.

[6] J. Bieker *et al.*, "Field emission characterization of *in situ* deposited gold nanocones with variable cone densities," *J. Vac. Sci. Technol. B Nanotechnol. Microelectron. Mater. Process. Meas. Phenom.*, vol. 36, no. 2, Jan. 2018, Art. no. 02C105.

[7] R. G. Forbes, C. J. Edgcombe, and U. Valdré, "Some comments on models for field enhancement," *Ultramicroscopy*, vol. 95, pp. 57–65, May/Jun. 2003.

[8] D. S. Roveri, G. M. Sant'Anna, H. H. Bertan, J. F. Mologni, M. A. R. Alves, and E. S. Braga, "Simulation of the enhancement factor from an individual 3D hemisphere-on-post field emitter by using finite elements method," *Ultramicroscopy*, vol. 160, pp. 247–251, Jan. 2016.

[9] D. Biswas, "Field-emission from parabolic tips: Current distributions, the net current, and effective emission area," *Phys. Plasmas*, vol. 25, no. 4, Apr. 2018, Art. no. 043105.

[10] G. S. Bocharov and A. V. Eletskii, "Effect of screening on the emissivity of field electron emitters based on carbon nanotubes," *Techn. Phys.*, vol. 50, no. 7, pp. 944–947, Jul. 2005.

[11] R. G. Forbes, "Physical electrostatics of small field emitter arrays/clusters," *J. Appl. Phys.*, vol. 120, no. 5, Aug. 2016, Art. no. 054302.

[12] J. R. Harris, K. L. Jensen, and D. A. Shiffler, "Dependence of optimal spacing on applied field in ungated field emitter arrays," *AIP Adv.*, vol. 5, no. 8, Aug. 2015, Art. no. 087182.

[13] D. Biswas, G. Singh, and R. Kumar, "Modeling field emitter arrays using nonlinear line charge distribution," *J. Appl. Phys.*, vol. 120, no. 12, Sep. 2016, Art. no. 124307.

[14] J. R. Harris, K. L. Jensen, J. J. Petillo, S. Maestas, W. Tang, and D. A. Shiffler, "Practical considerations in the modeling of field emitter arrays with line charge distributions," *J. Appl. Phys.*, vol. 121, no. 20, May 2017, Art. no. 203303.

[15] D. Biswas, "A universal formula for the field enhancement factor," *Phys. Plasmas*, vol. 25, no. 4, Apr. 2018, Art. no. 043113.

[16] T. A. de Assis, "Improving the extraction of characteristic field enhancement factors from nonlinear Fowler–Nordheim plots: Call for experimental tests," *J. Vac. Sci. Technol. B*, vol. 33, no. 5, Jul. 2015, Art. no. 052201.

[17] D. Biswas and R. Rudra, "Shielding effects in random large area field emitters, the field enhancement factor distribution, and current calculation," *Phys. Plasmas*, vol. 25, no. 8, Aug. 2018, Art. no. 083105.

[18] F. H. Read and N. J. Bowring, "Field enhancement factors of random arrays of carbon nanotubes," *Nucl. Instrum. Methods Phys. Res. A Accelerators Spectrometers Detectors Assoc. Equip.*, vol. 519, nos. 1–2, pp. 305–314, Feb. 2004.

[19] J.-M. Bonard *et al.*, "Tuning the field emission properties of patterned carbon nanotube films," *Adv. Mater.*, vol. 13, no. 3, pp. 184–188, Feb. 2001.

[20] T. A. de Assis and F. F. Dall'Agnol, "Evidence of universal inverse-third power law for the shielding-induced fractional decrease in apex field enhancement factor at large spacings: A response via accurate Laplace-type calculations," *J. Phys. Condens. Matter*, vol. 30, no. 19, Apr. 2018, Art. no. 195301.

[21] H. C. Miller, "Influence of gap length on the field increase factor $\beta$of an electrode projection (whisker)," *J. Appl. Phys.*, vol. 55, no. 1, pp. 158–161, Jan. 1984.

[22] E. G. Pogorelov, Y.-C. Chang, A. I. Zhbanov, and Y.-G. Lee, "Corrected field enhancement factor for the floating sphere model of carbon nanotube emitter," *J. Appl. Phys.*, vol. 108, no. 4, Aug. 2010, Art. no. 044502.

[23] J. R. Harris, K. L. Jensen, D. A. Shiffler, and J. J. Petillo, "Shielding in ungated field emitter arrays," *Appl. Phys. Lett.*, vol. 106, no. 20, May 2015, Art. no. 201603.

[24] S. N. Chiu, D. Stoyan, W. S. Kendall, and J. Mecke, "Point processes I—The Poisson point process," in *Stochastic Geometry and Its Applications*. New York, NY, USA: Wiley, 2013, pp. 35–63.

[25] R. H. Good, Jr., and E. W. Müller, *Field Emission* (Handbuch der Physik), vol. 21, S. Flügge, Ed. Berlin, Germany: Springer, 1956, pp. 176–231.

[26] P. A. Anderson, "Work function of gold," *Phys. Rev.*, vol. 115, no. 3, pp. 553–554, Aug. 1959.

[27] E. L. Murphy and R. H. Good, "Thermionic emission, field emission, and the transition region," *Phys. Rev.*, vol. 102, no. 6, pp. 1464–1473, Jun. 1956.

[28] R. E. Burgess, H. Kroemer, and J. M. Houston, "Corrected values of Fowler–Nordheim field emission functions $v(y)$ and $s(y)$," *Phys. Rev.*, vol. 90, no. 4, pp. 515–515, May 1953.

[29] R. G. Forbes, "Extraction of emission parameters for large-area field emitters, using a technically complete Fowler–Nordheim-type equation," *Nanotechnology*, vol. 23, no. 9, 2012, Art. no. 095706.

[30] K. L. Jensen, "Field emission—Fundamental theory to usage," in *Wiley Encyclopedia of Electrical and Electronics Engineering*. New York, NY, USA: Amer. Cancer Soc., Mar. 2014, pp. 1–29.

[31] S. H. Jo, Y. Tu, Z. P. Huang, D. L. Carnahan, D. Z. Wang, and Z. F. Ren, "Effect of length and spacing of vertically aligned carbon nanotubes on field emission properties," *Appl. Phys. Lett.*, vol. 82, no. 20, pp. 3520–3522, May 2003.

[32] J. Illian, A. Penttinen, H. Stoyan, and D. Stoyan, *Statistical Analysis and Modelling of Spatial Point Patterns*. New York, NY, USA: Wiley, 2008.

[33] T. A. de Assis and F. F. Dall'Agnol, "Minimal domain size necessary to simulate the field enhancement factor numerically with specified precision," *J. Vac. Sci. Technol. B*, vol. 37, no. 2, Feb. 2019, Art. no. 022902.

[34] R. C. Smith and S. R. P. Silva, "Maximizing the electron field emission performance of carbon nanotube arrays," *Appl. Phys. Lett.*, vol. 94, no. 13, Mar. 2009, Art. no. 133104.

[35] F. H. Read and N. J. Bowring, "Field enhancement factors of one-dimensional and two-dimensional arrays of nanotubes," *Microelectron. Eng.*, vols. 73–74, pp. 679–685, Jun. 2004.

JOHANNES BIEKER was born in Olpe, Germany, in 1991. He received the B.Sc. degree in physics from the University of Siegen in 2013 and the M.Sc. degree in physics from Technische Universität Dortmund in 2015, where he is currently pursuing the Doctoral degree with the Department of Electrical Engineering and Information Technology and he has been a Research Associate since 2015. His main research interest is micro–nano-integration and the development of vacuum gauges based on field emission.

RICHARD G. FORBES received the degree in theoretical physics from Trinity College, Cambridge, the B.A., M.A., and Ph.D. degrees from Cambridge University, and the D.Sc. degree from the University of Aston, Birmingham, U.K.

He has been officially retired for over 10 years, but remains located at the University of Surrey, U.K., Advanced Technology Institute, and remains highly research active, mainly in field electron emission (FE), but also in some aspects of field ion emission, electrostatics, and electrical thermodynamics. A theme behind much recent work has been to put the theory of the high-field technologies—particularly FE-based technologies—onto a better scientific basis. His research is "High Electric Field Nanoscience," especially, the theories of field electron and ion emission and related technologies. This area of technical physics lies between theoretical physics, electronic engineering, and materials science.

Dr. Forbes is a Professional Engineer (U.K. and European), a member of AVS, a Foreign Member of the Russian Academy of Natural Sciences (a Russian "civic society" organization), and an Inaugural Fellow of the International Field Emission Society (IFES). He served two terms as the IFES President. He has been the Chairman of the U.K. Engineering Council Surrey Region and Surrey SATRO (a local school support organization).

STEFAN WILFERT received the degrees in physics and in vacuum physics, and the Dr.rer.nat. degree (Ph.D.) from the Otto-von-Guericke-Universität Magdeburg. Since 2004, he has been a Research Assistant with the GSI Helmholtz Center for Heavy Ion Research, Darmstadt, Germany. In his function as a Work Package Leader, he is responsible for the development and design of the entire vacuum system of the new superconducting heavy ion synchrotron SIS100, the main accelerator of the Facility for Antiproton and Ion Research complex, which is being built as an extension of the existing GSI plant. He is a member of the American Vacuum Society and a referee for various international vacuum science-related journals.

HELMUT F. SCHLAAK was born in Berlin, Germany. He received the Dipl.-Ing. degree in electrical engineering and the Dr.-Ing. (Ph.D.) degree from the Technische Universität Berlin, Germany, in 1978 and 1984, respectively, with a thesis focused on integrated optical waveguide modulators. From 1983 to 1986, he was the Head of the Integrated Optics Group, Fraunhofer-Institute for Physical Measurement Techniques, Freiburg, Germany, where he was involved in research on integrated optic circuits for sensor systems. From 1986 to 1998, he was with Siemens AG, Berlin, in different leading positions. He was involved in research on microsensors, inkjet print heads, fiberoptic components, and new relay technologies. Since 1999, he has been a Full Professor with the Technische Universität Darmstadt, Darmstadt, Germany. His research interests include micro–nano-integration technologies, 3-D MEMS, microactuators, electroactive polymer actuators, piezoelectric actuators, and medical devices. He was a recipient of the Siemens Innovation Award for inventing a new silicon MEMS relay in 1997, and the VDE Ehrenring (Honorary Ring)—the Highest German Award in the field of Electrical Engineering, Electronics and Information Technology in 2018. He is Life Member of acting in different functions in the VDE and the VDE/VDI Society on Microelectronics, Microsystem Technology and Precision Engineering (GMM). He is a referee for several technical journals and conferences and the Chairman of various conferences and workshops.